The Texture of Rocks in the Earth's Deep Interior: Part II. Application of Texturing to the Deep Earth

1. Seismic Anisotropy

The Earth is composed of compositionally distinct units with characteristic properties. They are summarized in Fig. 1, which also gives information on temperature and pressure. The crust shows the greatest diversity of minerals (over 3000) that are accessible to direct observation in igneous, metamorphic, and sedimentary rocks. Emphasis of this review is the mantle and the solid inner core of the Earth. The Mg_2SiO_4 phase diagram covers the main phases in the mantle, olivine in the upper mantle, spinel-like structures ringwoodite and wadsleyite in the transition zone, perovskite ($MgSiO_3$), and periclase (MgO) in the lower mantle (Fig. 2). At higher pressure, phases tend to have simpler crystal structures than minerals in the crust, as established by high-pressure experiments and theory (e.g., Fiquet 2001). Particularly, phase transformations in the transition zone (400–700 km) are associated with large volume changes and this may be the cause of deep-focus earthquakes (Green and Houston 1995). The phase diagram for iron (Fig. 3) pertains to the core. In the solid inner core hexagonal (ε) iron is the most likely phase. What do we know about the deformation behavior of those minerals and how do they contribute to seismic anisotropy? But before investigating plasticity of mantle minerals, a brief discussion of anisotropic regions in the Earth is appropriate.

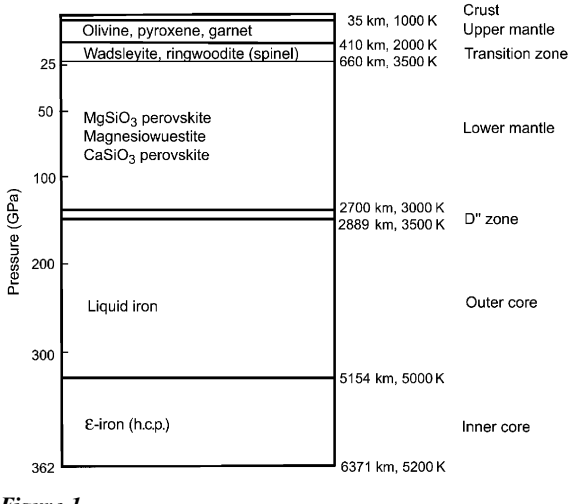

Figure 1
Structure of Earth. Depth, pressure, and temperature are indicated as well as main phases in the different units.

Seismic anisotropy was first recorded in the shallow upper mantle beneath Hawaii (Hess 1964, Morris *et al.* 1969), observing that surface waves travel $\sim$10% faster in the E–W direction than N–S. Since then maps of azimuthal anisotropy have been constructed for the uppermost mantle beneath oceanic lithosphere (e.g., Tanimoto and Anderson 1985; Fig. 4). Fast wave propagation directions overall correspond to flow directions as implied from plate motions. (This was the rationale for the original concept of Hess that [100] slip directions of olivine align with flow lines.) The anisotropy pattern has been refined and it became apparent that anisotropy in the upper mantle varies greatly with depth (e.g., Montagner and Guillot 2002). Overall, anisotropy at 200 km is much weaker than at 100 km. Beneath continents, anisotropy has been studied mainly with SKS body waves (waves that pass through the outer core and cross the mantle at a high angle). These S-waves become polarized in anisotropic media and the time differences between the fast and the slow wave arrivals are indicative of the degree of anisotropy (shear wave splitting). Anisotropy is at a deeper level beneath continents than oceans and less pronounced. It has been associated with tectonic processes and mountain building (e.g., Savage 1999, Silver 1996).

Anisotropy was documented in layers of the transition zone (400–700 km) where olivine breaks down to high-pressure phases. Particularly, just above the 660 km discontinuity anisotropy is pronounced and may be related to intense deformation near those phase transitions (Trampert and Heijst 2002). But contrary to the regular pattern of anisotropy in the uppermost mantle, anisotropic regions in the transition zone are confined, vary in extent and depth, and are to some degree associated with subduction (Fouch and Fischer 1996).

There is little evidence for anisotropy between 700 km and 2700 km (a few exceptions have been noted by Barruol and Hoffmann 1999), but this may be partially due to limited crossing ray coverage. However, the deep mantle, in the vicinity of the boundary with the core (D″ layer), reveals itself as a fascinating and heterogeneous area of the Earth (e.g., Kellogg *et al.* 1999). Geodynamic modeling suggests very strongly deformed subducting slabs (McNamara *et al.* 2001) and seismologists have observed anisotropy that could be due to texturing (e.g., Fouch *et al.* 2001, Kendall and Silver 1996, Ritsema 2000, Thomas and Kendall 2002, Vinnik *et al.* 1998), periodic layering (Garnero 2000), or partial melt (Lay *et al.* 1998). In most cases of mantle anisotropy, only the azimuthal variation of anisotropy is known and little information exists about the tilt, for example, of the fast propagation direction.

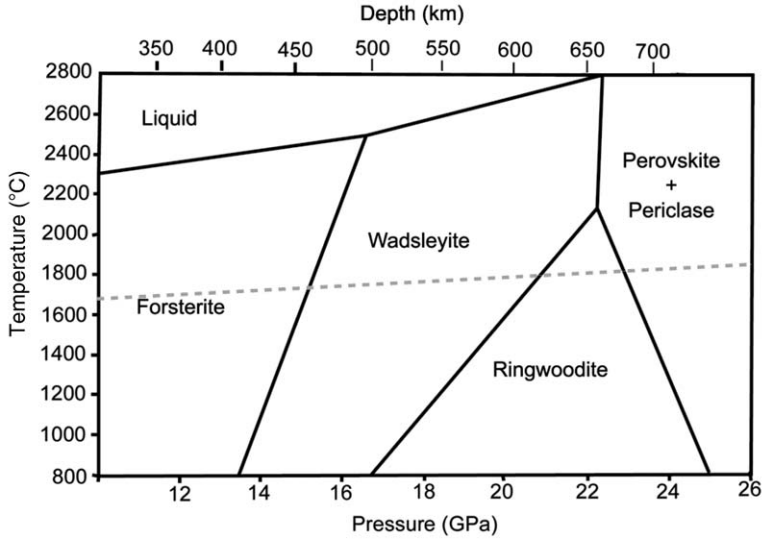

Figure 2
Pressure–temperature phase diagram for Mg_2SiO_4 (Cordier 2002). Approximate geotherm is indicated by dashed line.

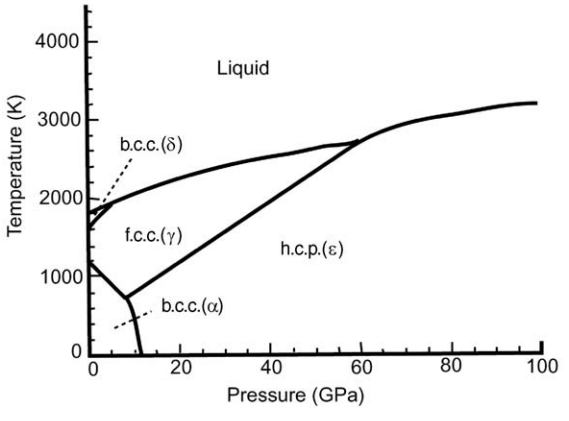

Figure 3
Pressure–temperature phase diagram for iron (Shen *et al.* 1998).

The outer core is liquid and thus isotropic, but it is firmly established, both from body waves and free oscillation observations, that the solid inner core is again anisotropic. Compressional P-waves travel 3–4% faster along the (vertical) axis of the Earth, than in the equatorial plane (e.g., Creager 1992, Romanowicz *et al.* 1996, Shearer 1994, Song 1997). Anisotropy may be concentrated near the surface of the inner core (Tromp 1993) or in the deeper parts (Song and Helmberger 1995).

In the next section we will explore how texture analysis and polycrystal plasticity can help us understand the anisotropy patterns in the Earth.

2. *Anisotropy in the Upper Mantle (Olivine)*

The mantle is not exposed on the surface of the Earth. However, during tectonic activity, smaller and larger parts of upper mantle rocks have been locally juxtaposed within the crust and can be sampled. The rocks are mainly peridotite, composed largely of olivine and subordinate pyroxene. Locations where mantle peridotites can be sampled are in Oman (studied extensively by Boudier and Nicolas 1995), as inclusions in volcanic rocks from Africa and several other places. Olivine in these peridotites is strongly oriented and texture patterns have been compiled by Ben Ismail and Mainprice (1998). By far the most common texture type has (010) poles nearly perpendicular to the foliation plane and [100] axes subparallel to the lineation direction (Fig. 5(a)). A much more rare texture type with (100) poles perpendicular to the foliation and [001] parallel to the lineation (Fig. 5(b)) has been found in the Alps (Möckel 1969) and the Horoman complex in Japan (Furusho and Kanagawa 1999). The latter type may not have formed in the mantle but during crustal deformation at great depth (80–100 km), and relatively low temperature (Frese *et al.* 2003). Microstructures in these naturally deformed olivine rocks indicate that deformation was accompanied by recrystallization.

Deformation mechanisms in olivine can be studied in the laboratory. It has been established, mainly through single-crystal experiments in compression geometry, that at high temperature (010)[100] is the preferred slip system (e.g., Bai *et al.* 1989, Nicholas *et al.* 1973). At lower temperature (100)[001] slip and

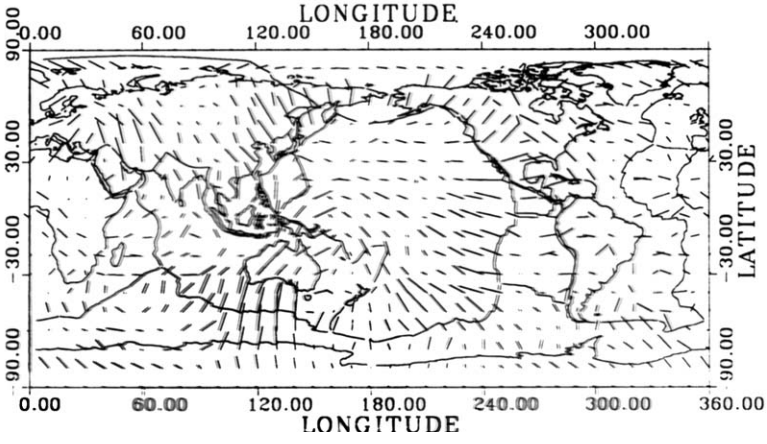

Figure 4
Distribution of velocities for Rayleigh waves. The lines correspond to the maximum velocities at a depth of ~100 km. Spreading ridges are indicated (Montagner and Tanimoto 1990).

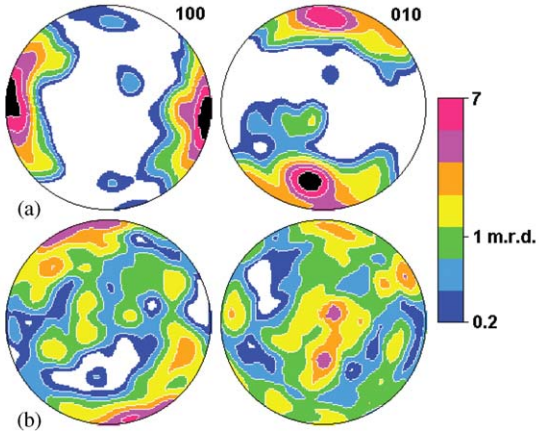

Figure 5
Texture types in naturally deformed olivine, represented as (100) and (010) pole figures. (a) High-temperature texture of peridotite from South Africa. This texture type is typical of mantle material. (b) Low-temperature texture in metamorphic olivinite from the deformed peripheral zone of the Alpe Arami ultramafic body, Central Alps; EBSP measurements, equal area projection, logarithmic contours.

{*hk*0}[001] pencil glide is dominant (Raleigh 1968). (100)[100] slip is also active at high temperature and high stress, with higher water content (Jung and Karato 2001). Slip systems were identified by optical and electron microscopy; critical resolved shear stresses, as well as strain rate sensitivities were determined in mechanical tests. These slip systems at higher and lower temperature are consistent with the two texture types shown in Fig. 5.

Knowing slip systems and their activity it should be possible to predict texture development for a given strain path. We will illustrate this by modeling olivine deformation and recrystallization with methods described in Part I. An olivine aggregate, with its low crystal symmetry and limited numbers of slip systems, is unlikely to deform homogeneously and a theory that is closer to equilibrium than compatibility is more realistic. For simple shear deformation, Fig. 6(b) shows (100) pole figures for pure deformation (with (010) slip dominating) and Fig. 6(d) for deformation accompanied by dynamic recrystallization (with nucleation dominating over boundary migration), with the self-consistent theory as a plasticity model. An asymmetric deformation texture, compatible with simple shear, transforms to a more symmetric recrystallization texture, with slip directions aligned in the shear direction. Those orientations nucleate preferentially because they are most highly deformed. The simulations are in excellent agreement with experiments (Zhang and Karato 1995), both for deformation (Fig. 6(a)) and recrystallization (Fig. 6(c)).

Since we can model a laboratory experiment, we can now apply the same method to the larger system of upper mantle deformation. In the mantle, large cells of convection are induced by instabilities and driven by temperature gradients (e.g., Bunge *et al.* 1998). The strain distribution in a convection cell is very heterogeneous but can easily be approached with polycrystal plasticity. On a microscopic scale, olivine is deformed in the upper mantle by intracrystalline processes such as slip of dislocations, and accompanying dynamic recrystallization. Dawson and Wenk (2000) have used the finite element method that incorporates as a constitutive equation polycrystal plasticity to investigate the development of

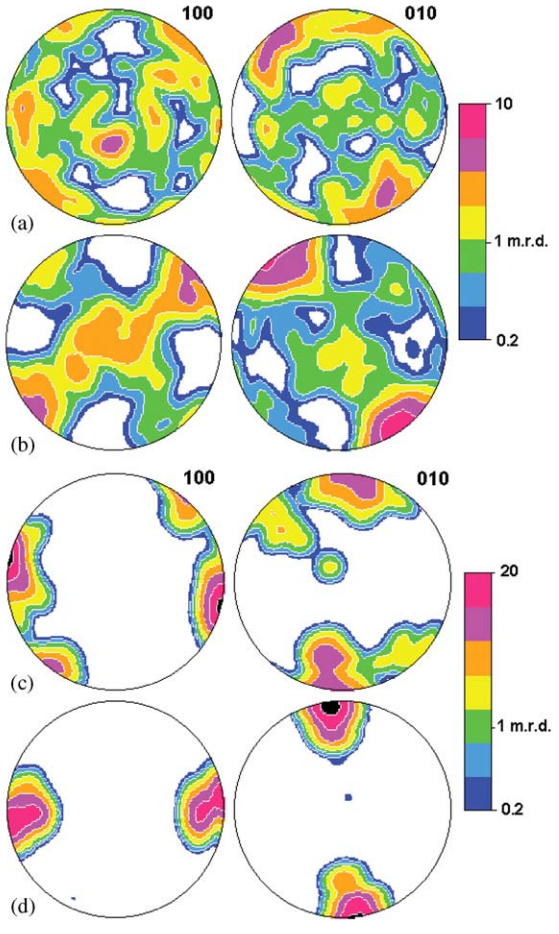

Figure 6
Texture types of olivine deformed in simple shear. (a, c) Experiments by Zhang and Karato (1995), (b, d) self-consistent simulations, assuming slip system activities representative of high temperature. (a, b) Pure deformation and (c, d) deformation accompanied by dynamic recrystallization; equal area projection, logarithmic contours (Wenk and Tome 1999).

anisotropy during mantle convection. Figure 7 follows texture development of olivine in the upper mantle along a streamline in (100) pole figures. A strong texture develops rapidly during upwelling (B). The preferred orientation stabilizes during spreading (C, D) and attenuates during subduction (E). The pole figures are distinctly asymmetric due to the component of simple shear. While the finite strain along a streamline increases monotonically, the texture does not. The map of textures in a hypothetical two-dimensional convection cell documents great heterogeneity (Fig. 8), both laterally and with depth. Texture development in the mantle is a highly dynamic process, which Wenk *et al.* (1999) tried to capture in a video.

Knowing texture patterns over the upper mantle, one can then average anisotropic elastic properties and from those evaluate seismic wave velocities. Figure 9 shows a map of compressional P-wave speeds in the vertical (i) and horizontal (ii) directions (Dawson and Wenk 2000). The map illustrates large variations, up to 15%, and reminds us of seismic tomographic maps of wave velocity variations that so far were mainly attributed to composition and temperature. Future geodynamic modeling as well as seismic interpretations should include the complexities of structural anisotropy and mechanical properties. All these factors have an influence of similar magnitude on wave velocities.

Even though in-detail texture development of olivine is complex and not simply an alignment of slip directions with flow lines, the overall seismic anisotropy of the uppermost mantle (Fig. 4) can be reasonably explained as a result of texturing during upwelling along ridges (Blackman *et al.* 2002).

3. *Lower Mantle*

Much less is known about the deeper Earth. Deformation experiments are more difficult because pressures are beyond conditions reached by ordinary mechanical devices. One approach has been to use analog systems with phases of similar structures and bonding but different compositions that are stable at lower pressure and deform at lower temperature. For example, for $MgSiO_3$ perovskite $CaTiO_3$ has been used (Karato *et al.* 1995). An analog for periclase (MgO) and magnesiowuestite ($FeMgO_2$) is halite (NaCl). But analogs are of questionable value when it comes to deformation mechanisms, since slip systems depend on the detailed electronic structure and bonding characteristics. Therefore, new deformation apparatuses are presently under development to deform single crystals and polycrystals at pressures up to 30 GPa (Durham *et al.* 2002). In some cases high-pressure phases can be recovered metastably and analyzed, for example, by electron microscopy, to establish active slip systems (e.g., review by Cordier 2002).

For nonquenchable phases, *in situ* observations are required and here texture comes to play a crucial role because, contrary to microstructure, texture can be measured at high pressure. If we know texture patterns, we can infer deformation mechanisms. With radial diamond anvil experiments, introduced in Part I, texture development in axial deformation can be studied at pressure above 400 GPa. Figure 10(a) is an inverse pole figure for MgO deformed at 47 GPa. The axial stress component is estimated to be 8.5 GPa. Materials such as MgO with NaCl structure deform on {111}, {110}, and {100} slip systems, all

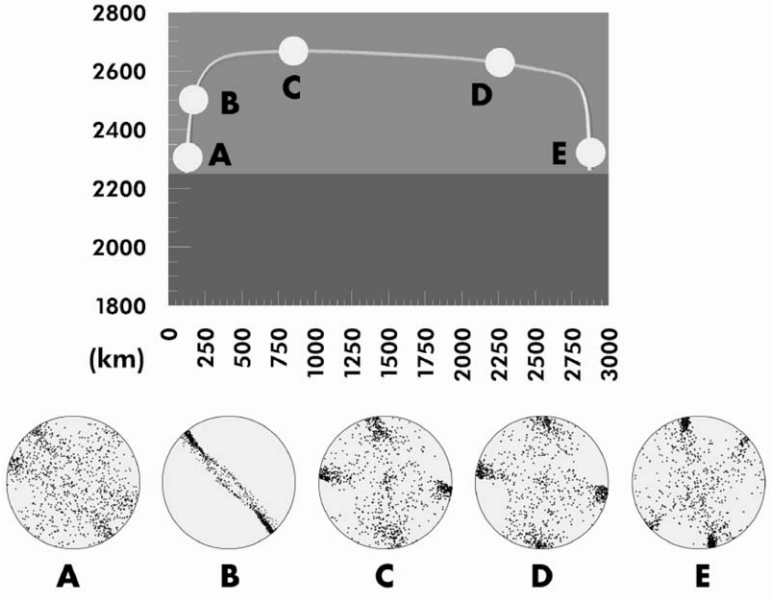

Figure 7
Mantle streamline with (100) olivine pole figures at five different locations.

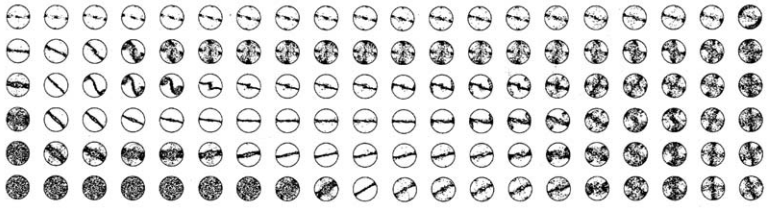

Figure 8
(100) pole figures of olivine at different locations in a simple mantle convection cell. Upwelling is on the left side, subduction on the right side (Dawson and Wenk 2000).

with the [110] slip direction (Carter and Heard 1970). In the case of NaCl, at low temperature {110} is favored but at higher temperature all systems operate with similar ease and the texture changes accordingly (Lebensohn *et al*. 2003). We illustrate for MgO how texture can be used to determine deformation mechanisms even if direct observation with an electron microscope is not possible (Merkel *et al*. 2002). The texture derived from the *in situ* diamond anvil diffraction experiment displays a strong (001) fiber component (Fig. 10(a)). This texture can only be simulated if exclusively {110} slip is active (Fig. 10(b)). If other slip systems are equally active (in Taylor simulations they are activated to maintain compatibility), the texture type is very different with a maximum at (110) (Fig. 10(c)). It can therefore be concluded that $\{110\}\langle 1\bar{1}0\rangle$ is the only significantly active slip system at 47 GPa and room temperature.

It is to be expected that at lower mantle conditions, in analogy to halite at higher temperature, several slip systems become active. Indeed, textures developed in high-temperature torsion experiments on magnesiowuestite by Stretton *et al*. (2001) and shear experiments by Yamazaki and Karato (2002) can only be explained by simultaneous activity of {111}, {110}, and {100} slip systems.

During subduction of upper mantle slabs into the lower mantle, geodynamic modeling suggests heterogeneous deformation with complicated streamlines (Kellogg *et al*. 1999, McNamara *et al*. 2001; Fig. 11). Using slip systems that were active in the high-temperature torsion experiments, we can then again predict texture evolution along a streamline in the subducting slab with increasing depth (Fig. 12). Simulated textures for MgO (represented as (100) pole figures) are strong at depths of 2000 km, but to

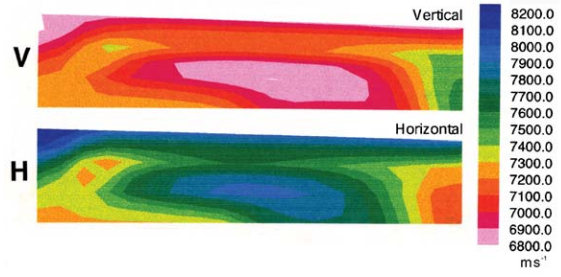

Figure 9
Seismic P-wave velocities in the mantle convection cell (Fig. 8), indicated by color pattern: (i) vertically traveling waves and (ii) horizontally traveling waves (Dawson and Wenk 2000).

produce seismic anisotropy, also substantial single-crystal elastic anisotropy is required. At high pressure and temperature, MgO is strongly anisotropic (e.g., Karki *et al*. 1999). Diamond anvil experiments, based on lattice distortions, also provide information on elastic properties at high pressure (Part I, fig. 5). Curiously, at intermediate pressures single-crystal anisotropy of MgO is minimal, which may explain absence of significant anisotropy in the intermediate lower mantle.

So far no convincing deformation experiments have been done with silicate perovskite. Experiments on the analog $CaTiO_3$ suggest that, while twinning may produce a texture at low temperature, at higher temperature superplasticity may be active with no preferred orientation (Karato *et al*. 1995). In diamond anvil experiments on silicate perovskite no texture was observed (Merkel *et al*. 2003a). Naturally there is uncertainty with such conclusions from samples with very small grain size. In the future, experiments need to be done with large samples, realistic size distributions, and compositions corresponding to those present in the lower mantle. Nevertheless, the large strains produced near the core mantle boundary, high-temperature gradients,

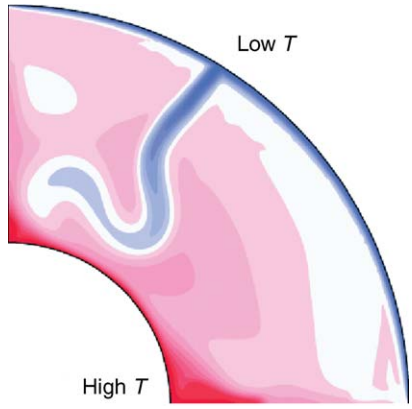

Figure 11
Temperature distribution during simulated subduction of a slab into the lower mantle (blue: cold, white: medium, red: hot, as indicated) (McNamara *et al*. 2001).

and conceivably phase transformations are likely to produce crystal preferred orientation, consistent with seismic observations of heterogeneity and anisotropy. While great progress is being made to better understand plasticity at high pressure, knowledge about deformation mechanisms of lower mantle phases at relevant conditions is still poor.

4. Core

The main component of the inner core is an iron-rich alloy, most likely with a hexagonal close-packed (h.c.p.) (ε-iron) structure (e.g., experiments by Shen *et al*. 1998, and first principles calculations by Wasserman *et al*. 1996).

As was mentioned earlier seismic waves travel ~3–5% faster along the NS axis of the inner core than in the equatorial plane (Fig. 13). There is general agreement that the reason for seismic anisotropy is an alignment of crystals but there are many ideas about the processes that lead to such an alignment. Wenk *et al*. (2000b) presented a model for core texturing

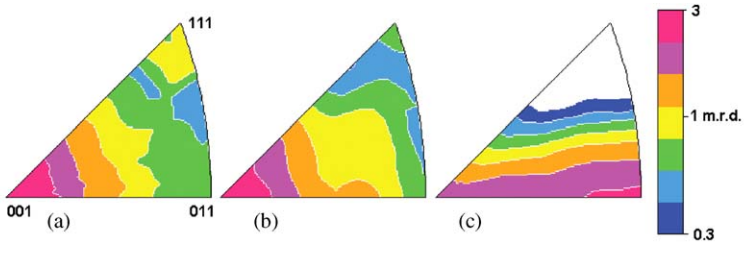

Figure 10
Inverse pole figures for MgO, deformed in axial compression. (a) *In situ* diamond anvil experiment at 20 GPa. To the right are simulations with {110}[1$\bar{1}$0] slip highly favored with (b) the self-consistent theory and (c) the Taylor theory (Merkel *et al*. 2002). Logarithmic contours.

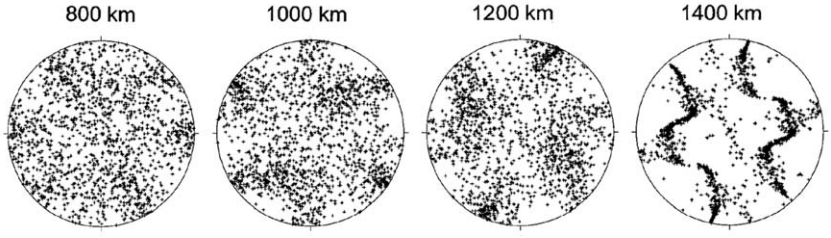

Figure 12
Simulation of texture development of periclase (MgO) during slab subduction into the lower mantle along a streamline of the McNamara *et al*. (2001) model at four different depths ({100} pole figures). It is assumed that {110} and {111) slip are equally active.

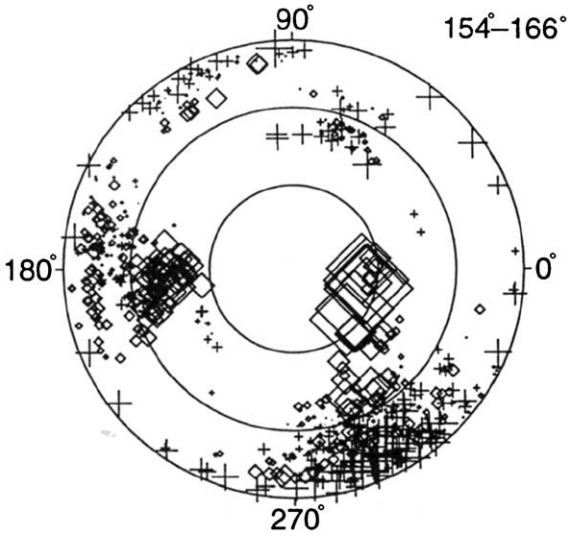

Figure 13
Inner core anisotropy. Plotted are ray residuals on a map with diamonds indicating negative (fast) residuals and crosses positive (slow) residuals. Symbol size is proportional to absolute value. North pole is in the center (Shearer 1994).

during convection. The quantitative analysis revealed that indeed strong textures would develop but, since temperature gradients are very small, internal radioactive heating would be required to drive convection. This is possible if potassium, which shows an affinity to iron at high pressure, is enriched in the core. Yoshida *et al*. (1996) propose growth in a stress field to minimize the free energy of the system. Another possibility is solidification texturing at the boundary with the liquid outer core (Bergman 1997). Finally, the Earth's magnetic field may produce stresses that deform the material and thus produce crystal rotations (Buffett and Wenk 2001, Karato 1999). Since the core is so remote, and many conditions are poorly known, convincing cases can be made for each mechanism.

Here we will only illustrate the example of the magnetic field. The largest electromagnetic (Maxwell) shear stresses in the Earth's geodynamo arise from the combined influence of the radial and azimuthal components of the magnetic field and are on the order of several Pa. Strain gradually accumulates to $\sim 50\%$ as the inner core grows by solidification in 1 M.y. The azimuthal component of the Maxwell stress, which is about an order of magnitude larger than the radial component, imposes a strong simple shear deformation.

A prerequisite for modeling this deformation is the knowledge about slip systems that are active in ε-iron. This phase is not stable at ambient conditions and deformation experiments need to be performed at high pressure. This can be done with diamond anvil cells, and again a comparison of texture patterns that were observed at pressures close to those in the inner core (220 GPa) (Fig. 14(a)) with polycrystal plasticity simulations (Fig. 14(b)) can be used to determine slip systems (Wenk *et al*. 2000a, 2000b). A strong *c*-axis maximum near the compression direction is only compatible with significant basal slip, consistent with *ab initio* predictions (Poirier and Price 1999). In this context the issue of inherited texture during phase transformations is significant (Merkel *et al*. 2003b). The deformation experiments start with α-iron (b.c.c.) and in compression two fibers, 001 and 110, develop (Fig. 15(a)). At 15 GPa the material transforms to ε-iron (h.c.p.) with a maximum at $(11\bar{2}0)$ (Fig. 15(b)). This is consistent with the Burgers (1934) relationship $(0001)\langle 11\bar{2}0\rangle$ (h.c.p.) and $\{110\}\langle 1\bar{1}1\rangle$ (b.c.c.) based on structural similarities of the b.c.c. and h.c.p. lattices. Upon further deformation in the ε-iron field this transformation texture changes by slip and the maximum moves to (0001) (Fig. 14(a)).

With such information about intracrystalline mechanisms, one can then apply the Maxwell stresses to the solid core and predict orientation patterns for different locations. Indeed, a strong texture develops,

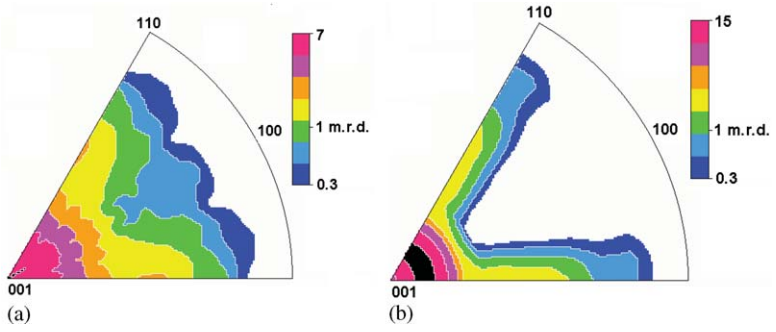

Figure 14
Inverse pole figures for ε-iron (h.c.p.) deformed in compression. (a) *In situ* diamond anvil texture determination at 220 GPa. (b) Texture simulation with the self-consistent theory for conditions that favor basal slip, 50% strain. Equal area projection, logarithmic contours (Wenk *et al*. 2000a, 2000b).

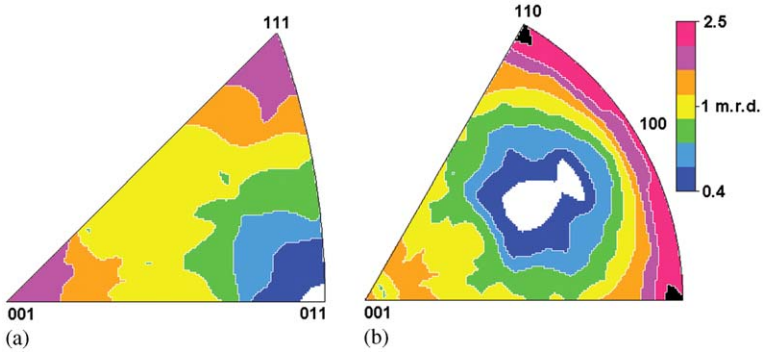

Figure 15
Inverse pole figures illustrating texture correspondence during the phase transformation from α-iron (b.c.c.) to ε-iron (h.c.p.) with increasing pressure: (a) is at 12.7 GPa and (b) at 21 GPa. Equal area projection, logarithmic contours (Merkel *et al*. 2003b).

particularly in the outer parts of the inner core (Buffett and Wenk 2001). A next step is to average single-crystal elastic properties over the simulated orientation distributions. This is not trivial since elastic properties for ε-iron have not been measured experimentally at inner core conditions. Until recently it was assumed that the fast P-wave propagation direction is parallel to the crystal *c*-axis (Fig. 16(a)), based on *ab initio* predictions for 0 K. A big surprise came when new calculations of Steinle-Neumann *et al*. (2001) included temperature and found that at core temperature (6000 K) the pattern is reversed, with fastest P-wave velocities perpendicular to the *c*-axis (Fig. 16(b)). For the Buffett and Wenk (2001) model, strong anisotropies are obtained for different locations (Figs. 16(c) and (d)), and if these patterns are averaged by applying axial Earth symmetry, one obtains a small anisotropy with faster velocities parallel to the N–S axis. Admittedly there are many uncertainties and the humble Francis Birch (1952) axiom that "Unwary readers should take warning that ordinary language undergoes modification to a high pressure form, when applied to the interior of the Earth, e.g., *Certain* (high pressure form)—*Dubious* (Ordinary meaning); *Undoubtedly*—*Perhaps; Positive proof*—*Vague suggestion*" is still valid and many arguments about the center of the Earth remain speculations in the realm of Jules Vernes. Several different processes may contribute to anisotropy. But the example illustrates that even for such remote places as the center of the Earth a combination of experimental techniques and theories that are commonly applied in materials science can be used to better understand structural features.

5. *Conclusions*

The discussion has illustrated that texture evolution and anisotropy in the Earth are complex and

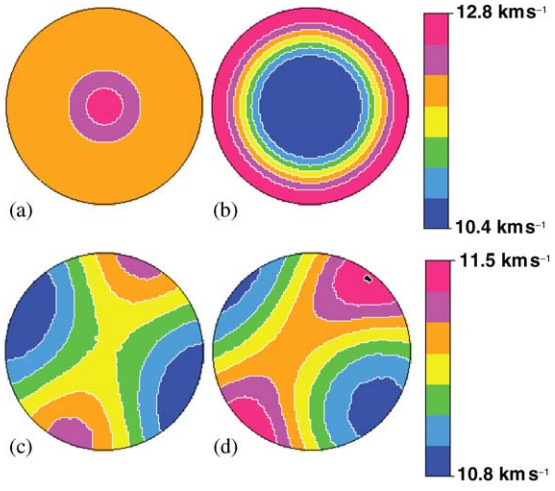

Figure 16
Anisotropy of ε-iron in the inner core shown as contoured P-velocity surfaces. (a, b) Single crystal P-velocities for ε-iron (h.c.p.), *c*-axis is in center (Steinle-Neumann *et al*. 2001): (a) 0 K and (b) 4000 K. (b, c) P-velocities for two locations near the surface of the inner core that was deformed and textured by Maxwell stresses. Equal area projection, linear contours (Buffett and Wenk 2001).

heterogeneous. Methods do exist to simulate patterns for a range of conditions but much work remains to be done. Clearly, there is no simple answer to anisotropy in the Earth such as "fast directions align with the flow direction." Preferred orientation of minerals in rocks is an important aspect of their plastic behavior and advanced computational methods help to link microscopic mechanisms and macroscopic properties. From observed texture patterns we can infer deformation mechanisms. If mechanisms are known, we can predict anisotropy that should evolve in geodynamic situations and, in turn, use seismic observations of anisotropy to interpret deformation processes in the deep Earth. Much of the progress that has been achieved relies on close collaborations of Earth and materials scientists, and the author has been greatly inspired by a long and fascinating interaction with Gilles Canova, Paul Dawson, Fred Kocks, Carlos Tomé, and others.

Bibliography

Bai Q, Mackwell S J, Kohlstedt D L 1991 High temperature creep of olivine single crystals: I. Mechanical results for buffered samples. *J. Geophys. Res.* **96**, 2441–63

Barruol G, Hoffmann R 1999 Upper mantle anisotropy beneath the GEOSCOPE stations. *J. Geophys. Res.* **104**, 10757–74

Ben Ismaïl W, Mainprice D 1998 An olivine fabric database: an overview of upper mantle fabrics and seismic anisotropy. *Tectonophysics* **296**, 145–57

Bergman M I 1997 Measurements of the elastic anisotropy due to solidification texturing and the implication for the Earth's inner core. *Nature* **389**, 60–3

Birch F 1952 Elasticity and constitution of the Earth's interior. *J. Geophys. Res.* **57**, 227–86

Blackman D K, Wenk H-R, Kendall J-M 2002 Seismic anisotropy in the upper mantle: 1. Factors that affect mineral texture and effective elastic properties. *Geochem. Geophys. Geosys.* **3**, 101029

Boudier F, Nicolas A 1995 Nature of the Moho transition zone in the Oman ophiolite. *J. Petrol.* **36**, 777–96

Buffett B, Wenk H-R 2001 Texturing of the inner core by Maxwell stresses. *Nature* **413**, 60–3

Bunge H-P, Richards M A, Lithgow-Bertelloni C, Baumgardner J R, Grand S P, Romanowicz B 1998 Time scales and heterogeneous structure in geodynamic Earth models. *Science* **280**, 91–5

Burgers W G 1934 On the process of transition of the cubic-body-centered modification into hexagonal-close-packed modification of zirconium. *Physica* **1**, 561–86

Carter N L, Heard H C 1970 Temperature and rate-dependent deformation of halite. *Am. J. Sci.* **269**, 193–249

Cordier P 2002 Dislocations and slip systems of mantle minerals. In: Karato S-I, Wenk H-R (eds.) *Plastic Deformation in Minerals and Rocks*, Reviews in Mineralogy. Mineralogical Society of America, Vol. 51, pp. 137–79

Creager K C 1992 Anisotropy of the inner core from differential travel times of the phases PKP and PKIKP. *Nature* **356**, 309–14

Dawson P R, Wenk H-R 2000 Texturing of the upper mantle during convection. *Phil. Mag. A.* **80**, 573–98

Durham W B, Weidner D J, Karato S-Y, Wang Y 2002 New developments in deformation experiments at high pressure. In: Karato S-I, Wenk H-R (eds.) *Plastic Deformation in Minerals and Rocks*, Reviews in Mineralogy. Mineralogical Society of America, Vol. 51, pp. 21–49

Fiquet G 2001 Mineral phases of the Earth's mantle. *Z. Kristallogr.* **216**, 248–71

Fouch M J, Fischer K M 1996 Mantle anisotropy beneath northwest pacific subduction zones. *J. Geophys. Res.* **101**, 15987–6002

Fouch M J, Fischer K M, Wysession M E 2001 Lowermost mantle anisotropy beneath the Pacific: imaging the source of the Hawaiian plume. *Earth Planet. Sci. Lett.* **190**, 167–80

Frese K, Trommsdorff V, Kunze K 2003 Olivine [100] normal to foliation: lattice preferred orientation in prograde garnet peridotite formed at high H_2O activity, Cima di Gagnone (Central Alps). *Contrib. Mineral. Petrol.* **145**, 75–86

Furusho M, Kanagawa K 1999 Transformation-induced strain localization in a lherzolite mylonite from the Hidaka metamorphic belt of central Hokkaido, Japan. *Tectonophysics* **313**, 511–32

Garnero E J 2000 Lower mantle heterogeneity. *Ann. Rev. Earth Planet. Sci.* **28**, 509–37

Green H W, Houston H 1995 The mechanics of deep earthquakes. *Ann. Rev. Earth Planet. Sci.* **23**, 169–213

Hess H H 1964 Seismic anisotropy of the uppermost mantle under oceans. *Nature* **203**, 629

Jung H, Karato S 2001 Water-induced fabric transitions in olivine. *Science* **293**, 1460–3

Karato S-I 1999 Seismic anisotropy of the Earth's inner core resulting from flow induced by Maxwell stresses. *Nature* **402**, 871–3

Karato S-I, Zhang S, Wenk H-R 1995 Superplasticity in the Earth's lower mantle. Evidence from seismic anisotropy and rock physics. *Science* **270**, 458–61

Karki B B, Wentzcovitch R M, de Gironcoli S, Baroni S 1999 First principles determination of elastic anisotropy and wave velocities of MgO at lower mantle conditions. *Science* **286**, 1705–9

Kellogg L H, Hager B H, van der Hilst R D 1999 Compositional stratification in the deep mantle. *Science*. **283**, 1881–4

Kendall J M, Silver P G 1996 Constraints from seismic anisotropy on the nature of the lowermost mantle. *Nature* **381**, 409–12

Lay T, Williams Q, Garnero E J 1998 The core–mantle boundary layer and deep Earth dynamics. *Nature* **392**, 461–8

Lebensohn R A, Dawson P R, Wenk H-R, Kern H 2003 Heterogeneous deformation and texture development in halite: modelling with finite element and selfconsistent approaches, and experimental validation. *Tectonophysics* (in press)

McNamara A K, Karato S-I, van Keken P E 2001 Localization of dislocation creep in the lower mantle: implications for the origin of seismic anisotropy. *Earth Planet. Sci. Lett.* **191**, 85–99

Merkel S, Wenk H-R, Badro J, Montagnac J, Gillet P, Mao H K, Hemley R J 2003a Deformation of $(Mg_{0.9},Fe_{0.1})SiO_3$ perovskite aggregates up to 60 GPa. *Earth Planet. Sci. Lett.* **209**, 351–60

Merkel S, Wenk H-R, Shu J, Shen G, Gillet P, Mao H-K, Hemley R J 2003b Deformation of polycrystalline iron up to 30 GPa and 1000 K. *Phys. Earth Planet. Inter.* (submitted)

Merkel S, Wenk H-R, Shu J, Shen G, Gillet P, Mao H-K, Hemley R J 2002 Deformation of MgO aggregates at pressures of the lower mantle. *J. Geophys. Res.* **107**

Möckel J R 1969 Structural petrology of the garnet-peridotite of Alpe Arami (Ticino, Switzerland). *Leidse Geol. Med.* **42**, 61–130

Montagner J P, Guillot L (2002) Seismic anisotropy and global dynamics. In: Karato S-Y, Wenk H-R (eds.) *Plasticity of Minerals and Rocks*, Reviews in Mineralogy and Geochemistry. Mineralogical Society of America, pp. 353–85

Montagner J P, Tanimoto T 1990 Global anisotropy in the upper mantle inferred from the regionalization of phase velocities. *J. Geophys. Res.* **95**, 4797–819

Morris G B, Raitt R W, Shor G G 1969 Velocity anisotropy and delay time maps of the mantle near Hawaii. *J. Geophys. Res.* **74**, 4300–16

Nicholas A, Boudier F, Boullier A-M 1973 Mechanisms of flow in naturally and experimentally deformed peridotites. *Am. J. Sci.* **273**, 853–76

Poirier J-P, Price G D 1999 Primary slip system of epsilon-iron and anisotropy of the Earth's inner core. *Phys. Earth Panet. Inter.* **110**, 147–56

Raleigh C B 1968 Mechanisms of plastic deformation in olivine. *J. Geophys. Res.* **73**, 5391–406

Ritsema J 2000 Evidence for shear velocity anisotropy in the lowermost mantle beneath the Indian Ocean. *Geophys. Res. Lett.* **27**, 1041–4

Romanowicz B, Li X D, Durek J 1996 Anisotropy of the inner core: could it be due to low-order convection? *Science* **274**, 963–6

Savage M K 1999 Seismic anisotropy and mantle deformation. What have we learned from shear wave splitting? *Rev. Geophys.* **37**, 65–106

Shearer P M 1994 Constraints on inner core anisotropy from PKP(DF) travel times. *J. Geophys. Res.* **99**, 19647–59

Shen G, Mao H-K, Hemley R J, Duffy T S, Rivers M L 1998 Melting and crystal structures of iron at high pressures and temperatures. *Geophys. Res. Lett.* **25**, 373–6

Silver P G 1996 Seismic anisotropy beneath the continents: probing the depths of geology. *Ann. Rev. Earth Planet. Sci.* **24**, 385–432

Song X 1997 Anisotropy of the Earth's inner core. *Rev. Geophys.* **35**, 297–313

Song X, Helmberger D V 1995 Depth dependence of anisotropy in Earth's inner core. *J. Geophys. Res.* **100**, 9805–16

Steinle-Neumann G, Stixrude L, Cohen R E, Gülseren O 2001 Elasticity of iron at the temperature of the Earth's inner core. *Nature* **413**, 57–60

Stretton I, Heidelbach F, Mackwell S, Langenhorst F 2001 Dislocation creep of magnesiowuestite $(Mg_{0.8}Fe_{0.20})$. *Earth Planet. Sci. Lett.* **194**, 229–40

Tanimoto T, Anderson D L 1985 Lateral heterogeneity and azimuthal anisotropy of the upper mantle: Love and Rayleigh waves 100–250 s. *J. Geophys. Res.* **90**, 1842–58

Thomas C, Kendall J-M 2002 The lowermost mantle beneath northern Asia: II. Evidence for lower-mantle anisotropy. *Geophys. J. Int.* **151**, 296–308

Trampert J, Heijst H J 2002 Global azimuthal anisotropy in the transition zone. *Science* **296**, 1297–9

Tromp J 1993 Support for anisotropy of the Earth's inner core from free oscillations. *Nature* **366**, 678–81

Vinnik L, Breger L, Romanowicz B 1998 Anisotropic structures at the base of the Earth's mantle. *Nature* **393**, 564–7

Wasserman E, Stixrude L, Cohen R E 1996 Thermal properties of close-packed phases of iron at high pressures and temperatures. *Phys. Rev.* **B53**, 8296–309

Wenk H-R, Tomé C N 1999 Modeling dynamic recrystallization of olivine aggregates deformed in simple shear. *J. Geophys. Res.* **104**, 25513–27

Wenk H-R, Dawson P, Pelkie C, Chastel Y 1999 *Texturing of Rocks in the Earth's Mantle. A Convection Model Based on Polycrystal Plasticity*. Video. American Geophysical Union

Wenk H-R, Baumgardner J, Lebensohn R, Tomé C 2000a A convection model to explain anisotropy of the inner core. *J. Geophys. Res.* **105**, 5663–77

Wenk H-R, Matthies S, Hemley R J, Mao H-K, Shu J 2000b The plastic deformation of iron at pressures of the Earth's inner core. *Nature* **405**, 1044–7

Yamazaki D, Karato S 2002 Shear deformation of (Mg,Fe)O: implications for seismic anisotropy in Earth's lower mantle. *Phys. Earth Planet. Inter.* **131**, 251–67

Yoshida S, Sumita I, Kumazawa M 1996 Growth model of the inner core coupled with the outer core dynamics and the resulting elastic anisotropy. *J. Geophys. Res.* **101**, 28085–103

Zhang S, Karato S-Y 1995 Lattice preferred orientation of olivine aggregates deformed in simple shear. *Nature* **375**, 774–7

H.-R. Wenk

Encyclopedia of Materials: Science and Technology
ISBN: 0-08-043152-6
pp. 1–11